GEOPHYSICS, VOL. 66, NO. 4 (JULY-AUGUST 2001); P. 1002–1014, 10 FIGS.

A seismic and gravity study of the McGregor geothermal system, southern New Mexico

T. M. O'Donnell, Jr.*, K. C. Miller‡, and J. C. Witcher**

ABSTRACT

Seismic and gravity studies have proven to be valuable tools in evaluating the geologic setting and economic potential of the McGregor geothermal system of southern New Mexico. An initial gravity study of the system demonstrated that a gravity high coincides with the heat-flow high. A subsequent seismic reflection survey images a strong reflector, interpreted to be associated with a bedrock high that underlies the gravity and heat-flow highs. A single reflection, which coincides with the water table, occurs within the Tertiary basin fill above bedrock. This reflector is subhorizontal except above structurally high bedrock, where it dips downward. This observation is consistent with well data that indicate a bedrock water table 30 m lower than water in the basin-fill aquifer. Velocity models derived from seismic tomography show that the basin fill has velocities in the range of 800 to 4000 m/s and that the bedrock reflector coincides with high velocities of 5000 to 6000 m/s. Low-velocity zones within the bedrock high are interpreted as karsted bedrock with solution-collapse breccias and cavities filled with hot water. Higher velocity material that flanks the bedrock high may represent an earlier stage of basin fill or older alluvial-fan deposits. The heat-flow anomaly appears to be constrained to the region of shallowest bedrock that lacks these deposits, suggesting that they may act as an aquitard to cap underlying bedrock aquifers or geothermal reservoirs. Taken together, these observations suggest that the geothermal system is associated with karsted and fractured structurally high bedrock that serves as a window for upwelling and outflow of thermal waters. Thermal waters with a temperature as high as 89°C have the potential for space heating, geothermal desalinization, and small-scale electrical production at McGregor Range.

INTRODUCTION

The McGregor system is one of 27 known convective hydrothermal systems within the southern Rio Grande rift (Witcher, 1988). These systems are primarily forced-convection systems in which groundwater is circulated to great depth, heated from elevated temperature conditions in the rift, returned to the surface, and discharged in favorable geologic settings (Harder et al., 1980; Witcher, 1988; Barrol and Reiter, 1990). Over the years, a number of these systems have been exploited for space heating and large commercial greenhouses and to produce small amounts of electricity (Witcher, 1988).

The McGregor geothermal system was first recognized through reports of hot water in wells drilled for stock water and potability evaluation (McLean, 1956). Further evaluation of the system, then known as the Hueco Tanks geothermal system, took place in the late 1970s when a number of geologic, temperature gradient, and geochemical studies of thermal waters were made in West Texas (Henry, 1979; Hoffer, 1979; Taylor et al., 1980; Henry and Gluck, 1981; Taylor, 1981). Recently, additional drilling and temperature gradient measurements have confirmed that the highest heat flow is on McGregor Range in southern New Mexico (Witcher, 1998). The McGregor geothermal system has estimated heat-flow values as high as 700 mW/m^2—much higher than the typical measurements for the southern Rio Grande rift of 85 to 123 mW/m^2 (Decker and Smithson, 1975; Reiter et al., 1975, 1978, 1979, 1986; Taylor and Roy, 1980; Morgan, 1989; Witcher, 1998).

The geothermal system is located near the U.S. Army's McGregor Range Base Camp in southern New Mexico. The military is interested in using this resource as a source of energy. A number of geological, geochemical, and geophysical studies were conducted from 1994 until 1998 to gain a better understanding of the geothermal system. Geologic mapping, a radon

Manuscript received by the Editor November 24, 1999; revised manuscript received November 14, 2000.
*Conoco Inc., 600 N. Dairy Ashford, Houston, Texas 77079-1175.
‡University of Texas at El Paso, Department of Geological Sciences, 500 W. University Ave., E1 Paso, Texas 79968-0555. E-mail: miller@geo.utep.edu.
**New Mexico State University, Southwest Technology Development Institute, Las Cruces, New Mexico 88003-3001. E-mail: jwticher@nmsu.edu.

soil gas survey, a soil mercury survey, and a shallow temperature gradient and heat-flow study (1) delineated the shallow thermal regime and possible upflow zones and (2) identified previously unknown structures (Witcher, 1998). These studies were followed by a detailed spontaneous potential (SP) survey (Ross and Witcher, 1995) and by gravity and seismic surveys (O'Donnell, 1998). Information from these efforts was then used to select deep slim-hole test sites (Finger and Jacobson, 1997; Witcher et al., 1997). Finally, geochemical sampling of deep well fluids (Witcher, 1998) and a dipole–dipole resistivity survey (Ross et al., 1998) were conducted to refine reservoir hydrogeology interpretations. Here, we present the results of the seismic and gravity study and integrate them with other work.

GEOLOGIC SETTING

The McGregor geothermal system is situated along the eastern margin of the Tularosa-Hueco basin (Figure 1), a major half-graben complex of the Rio Grande rift (Woodward et al., 1978; Seager and Morgan, 1979; Sinno et al., 1986). The Tularosa-Hueco half-graben is rotated down to the west along the East Franklin Mountains fault system (Seager, 1980; Machette, 1987; Collins and Raney, 1994). Interpretation of seismic and gravity data suggests that Cenozoic basin fill reaches 2750 m thick a few kilometers east of the East Franklin Mountains fault (Mattick, 1967; Collins and Raney, 1994). An en echelon series of northwest-trending normal faults deform basin fill from the East Franklin Mountains fault to the area of the McGregor geothermal system (Figure 1) (Seager, 1980; Seager et al., 1987; Buck et al., 1998). A north-trending Pleistocene fault zone, possibly related to the geothermal anomaly, was recently recognized just east of Davis Dome (Witcher, 1998) (Figure 2). The late Pleistocene fault zone is characterized by up to 15 m of total displacement as defined by geomorphic surface offsets with stage IV–V caliche (Gile et al., 1966; Machette, 1985) on the Camp Rice aggradational surface east of Davis Dome.

The basin fill unconformably overlies bedrock composed primarily of Paleozoic limestone and dolomite intruded by mid-Tertiary felsic sills and laccoliths. Several outcrops of Paleozoic limestone and mid-Tertiary intrusions occur within the study area, suggesting significant topography on the bedrock surface (Figure 2). Deep continuous-wireline core drilling encountered open fractures in nearly all bedrock units. Regionally, Silurian and Ordovician strata are known to contain very large zones of pre-Mississippian solution-collapse breccias (Lucia, 1988). Wells 45-5 and 46-6 (Figure 2), two of the deep core holes, encountered solution-collapse breccias in all Paleozoic units and water-filled cavernous intervals in Pennsylvanian limestones at or near the Tertiary basin-fill unconformity and adjacent to the static water level (Witcher et al., 1997). Mid-Tertiary felsite sills and laccoliths, encountered during core drilling, also show

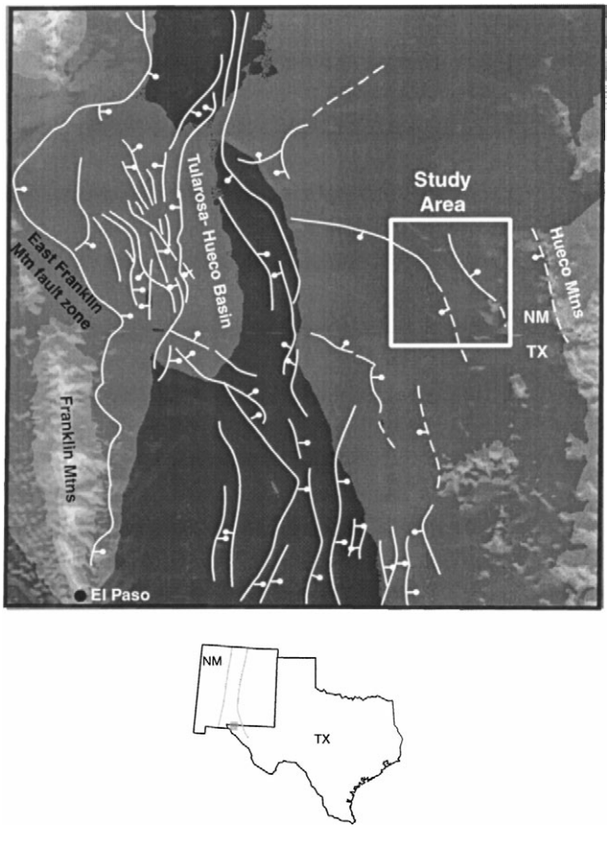

FIG. 1. The study area relative to topography and Tertiary normal faults of the Rio Grande rift. Faulting after Seager (1980). Dark shading indicates lower elevations; light shading indicates higher elevation. Inset locates map with respect to state boundaries and the rift boundaries (gray lines).

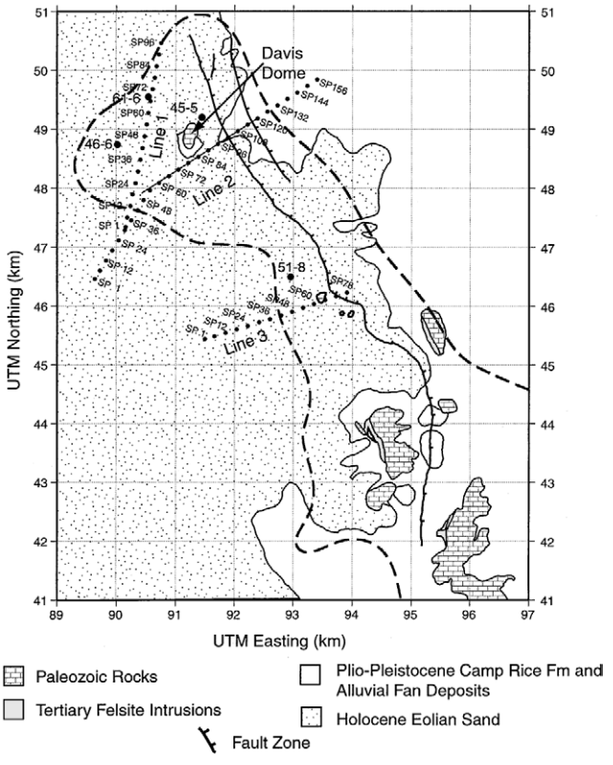

FIG. 2. Geologic map of the study area outlined in Figure 1. Large black circles—wells; gray line—resistivity profile; black dots—SP locations for seismic lines; dashed black line—400 mW/m^2 heat-flow contour.

intervals with open fractures. Localized solution and fracture permeability of bedrock permit upward circulation of geothermal waters from great depth and also channel shallow outflow laterally (Witcher, 1998).

The basin fill is composed of the late Tertiary Fort Hancock and Quaternary Camp Rice Formations (Stuart and Willingham, 1984; Gustavson, 1991). In this area, the Fort Hancock Formation consists of interbedded claystones, gypsiferous claystones, siltstones, and sandstones that were deposited in fluvial, lacustrine, and playa environments. The Camp Rice Formation unconformably overlies the Fort Hancock Formation in the Hueco-Tularosa basin (Stuart and Willingham, 1984; Gustavson, 1991). The Camp Rice Formation consists of ancestral Rio Grande fluvial-channel sand and flood-plain silt and clay beneath the basin floor and forms alluvial fans adjacent to the Hueco Mountains (Gustavson, 1991). The study area is mostly covered with a thin veneer of Holocene eolian deposits (Figure 2) (Blair et al., 1990; Buck et al., 1998). The Fort Hancock Formation is not a host for geothermal resources but does appear to locally confine or provide leaky caps over the geothermal systems as a result of its fine-grained composition.

SEISMIC REFLECTION DATA

Seismic data were collected across the heat flow high (Figure 2) to determine bedrock geometry associated with this anomaly and to image any faults that might be serving as conduits for rising hot water. Approximately 14.8 km of data were collected during the seismic survey along three profiles. One of the profiles, line 2, was occupied a second time to obtain longer offset data. The reflection data were collected in a 48-channel split-spread geometry with source and group intervals of 33.3 m. At each source location, four 0.149-kg boosters were fired independently in a four-hole pattern. Data were recorded for 2 s at a 1-ms sample rate. Maximum offsets reached 971 m as a result of asymmetries in the spread. During the reoccupation of line 2, offsets of 2761 m were achieved by shooting off-end of a 60-channel spread.

Preliminary processing of the data included a vertical stack of each shot in the four-hole pattern, geometry assignment, trace editing, application of elevation statics, and application of a 500-ms automatic gain control (AGC). Shot gathers from three locations on line 2 (Figure 3) show that the data are characterized by clean first arrivals, strong ground roll, and a prominent reflection at 400 to 700 ms on shots 29 and 129 that appears to be absent on shot 78. Since the data were dominated by ground roll below 20 Hz and had little coherent energy above 80 Hz, a 30–80-Hz band-pass filter was applied to the data. The filter effectively suppressed the ground roll but still did not bring out a reflector on SP 78. After velocity analysis, data were corrected for NMO and stacked. Smoothed versions of stacking velocity functions were used to produce depth-converted record sections.

All three stacked record sections (Figure 4) are characterized by a strong coherent reflector at 150 to 500 ms that is interpreted to be the top of bedrock. Few reflectors occur within the overlying basin fill except on line 2, where a discontinuous reflector at 150–250 ms is seen. Well data on the southwest end of the line suggest this is a reflection from the water table within the basin fill. The reflector is shallower to the north than to the south and either dips into or disappears at the bedrock high. On line 2 the bedrock reflector loses continuity where it steps up from 500 to 150 ms. This may be the result of faulting and/or a rough bedrock surface. This observation is consistent with the raw data for shot 78 (Figure 3), which lacked evidence of a prominent bedrock reflector.

VELOCITY MODELS FROM REFRACTION ANALYSIS

To supplement interpretation of the stacked record sections, velocity models were derived for each profile by inverting first

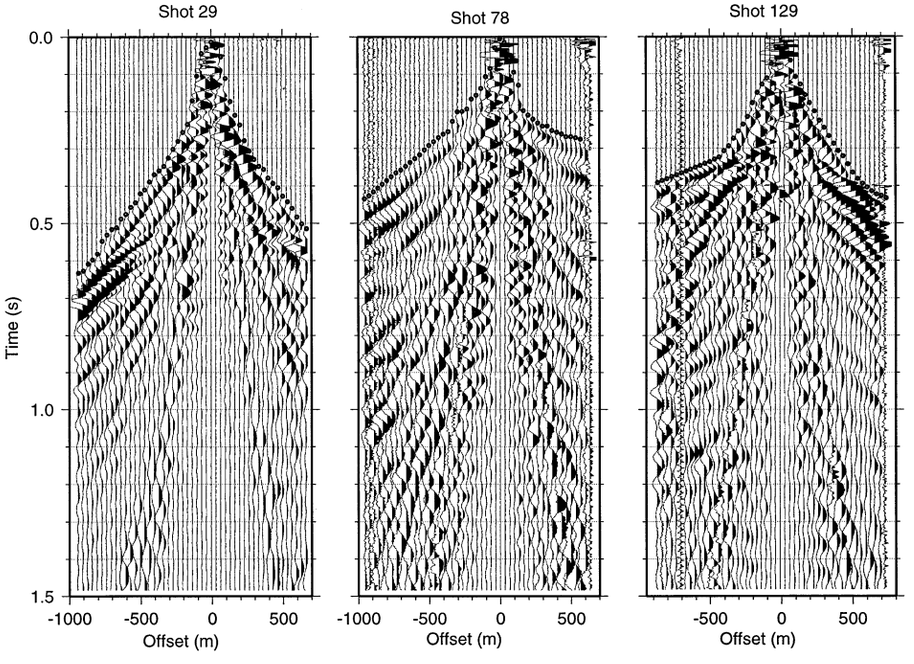

FIG. 3. Example shot gathers from the first deployment of line 2 showing first-arrival picks (black circles). First arrivals were picked at the onset of a trough.

arrivals in the shot data. Direct and refracted arrivals supply information on the near-surface rock velocity and aid in interpreting the subsurface geology by providing constraints on structure, lithology, and fluid saturation. Velocity models derived from first-arrival information are particularly helpful in estimating subsurface structure and lithology in the topmost 100 m, where the reflection data are often poor because of low fold, short traveltimes, and noise. Inversion schemes are well suited to reflection data sets because they take advantage of the many shots in a reflection survey to obtain high-resolution velocity models. To obtain velocity models for the shallow subsurface, first-arrival times for each seismic line were input into (1) Advance Geophysical's ProMAX turning-ray tomography package and (2) the first-arrival inversion of Ammon and Vidale (1993). Both methods yielded comparable results. Here we present the results from the Ammon inversion.

First arrivals

First-arrival times were picked at the onset of seismic energy, which, in this data set, is at the onset of a trough (Figures 3 and 5). As a rule, the first-arrival times were picked on unfiltered shot gathers, using a filtered gather for reference, to avoid apparent shifts in arrival times caused by band-pass filtering.

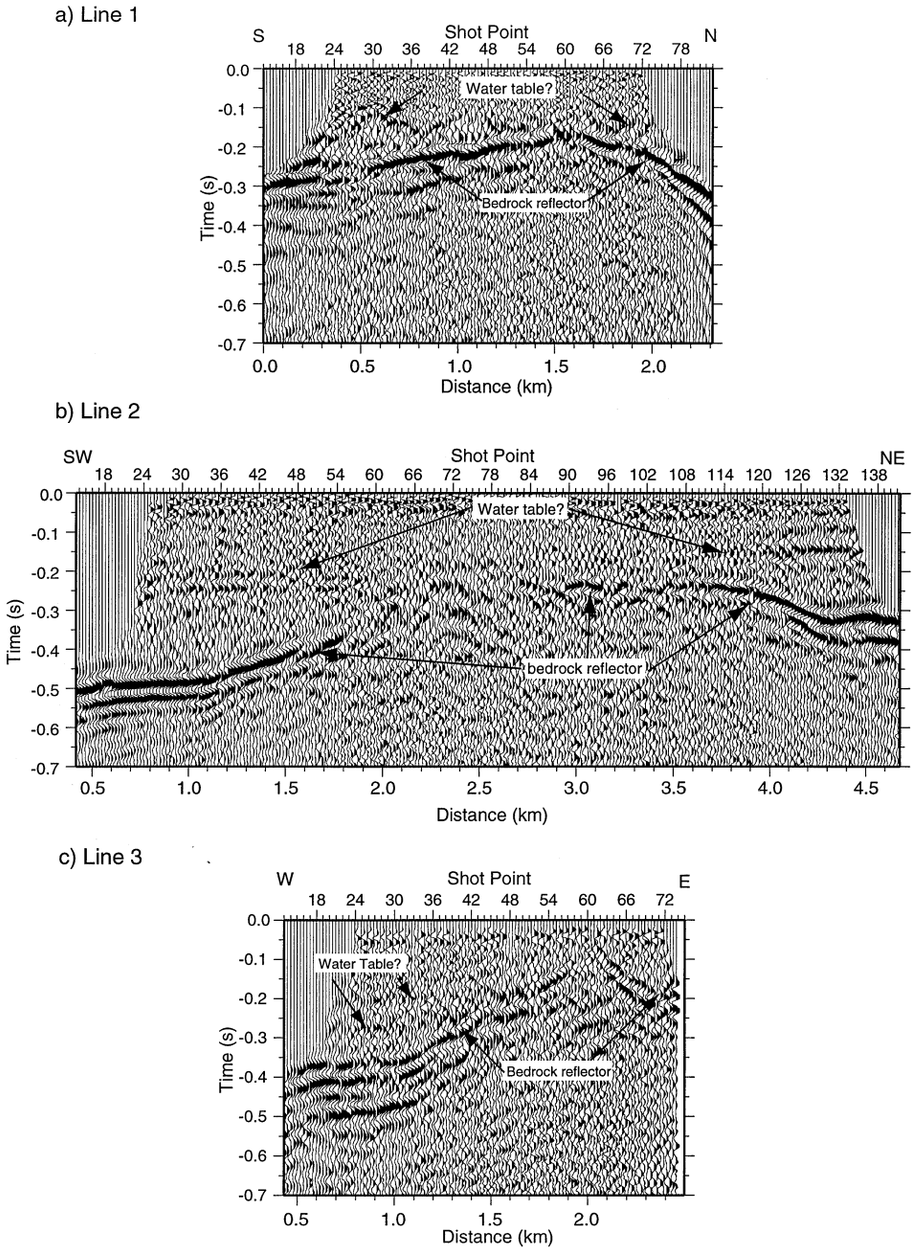

FIG. 4. Stacked record sections for (a) line 1, (b) line 2, and (c) line 3. Vertical exaggeration is approximately 2:1. The data have a continuous reflector present at 150–500 ms interpreted as bedrock. The reflector shallows as it crosses over the gravity and heat-flow high, suggesting a bedrock high coincident with these anomalies.

Preliminary analysis of first-arrival times on line 2 (Figure 3) suggests significant lateral velocity variations in the near surface. Low apparent velocities in the first arrivals indicate deeper bedrock at either end of the line, and high apparent velocities near the middle of the line suggest shallow bedrock. On shot 29 at the southwest end of the line, the first arrival at 700 m offset is at >500 ms (Figure 3). Toward the center of the line, on shot 78 (Figure 3) at 700 m offset, the first-arrival time decreases to 300–400 ms. To the northeast on shot 129, the arrival time at 700 m offset to the right of the source increases to >400 ms again. On the longer offset data (Figure 5) the first arrivals at offsets >700 m suggest even more structural complexity than seen at shorter offsets. On shot 15 at offsets of 800 to 1100 m (Figure 5), the first arrivals are nearly horizontal, indicating the presence of either extremely high-velocity material or high structural dips.

Inversion

First-arrival data were inverted to obtain velocity models along each profile using the tomographic method of Ammon and Vidale (1993). The procedure requires mechanisms for computing traveltimes, an initial velocity model, parameters for stabilizing the inversion, and a means for assessing model reliability. The velocity model is parameterized as a series of discrete constant-velocity cells. Traveltimes through the model are calculated using a finite-difference scheme to iteratively solve the eikonal equation for the position of the wavefront (Vidale, 1988, 1990). A Laplacian smoothness constraint is used to stabilize the inversion to ensure reasonable estimates of the final velocity model. The smoothness constraint parameter imposes a trade-off between model smoothness and the size of traveltime residuals and is determined by trial and error. The smoothing still allows for strong velocity contrasts by smoothing the total amount of slowness fluctuation in the model rather than individual slowness contrasts.

The tomography is an iterative procedure in which each iteration consists of a traveltime calculation and an inversion to find adjustments to the model. The velocity model output from one iteration is input into the next iteration. After each iteration, the rms traveltime residual is compared to the rms traveltime residual from the previous iteration. When the inversion ceases to make significant changes to the rms traveltime residual, calculations are stopped and the final velocity model is taken from the output of the last iteration.

In this paper we present ray coverage diagrams as one measure of resolution (Figure 6). In addition, checkerboard tests run on the final velocity models suggest that lateral resolution is better than vertical resolution.

Parameters chosen for this study included a cell size of 50 m for the velocity model. To ensure accuracy of the traveltime calculation, the model was subsampled to 7-m cells. For lines 1 and 3, the inversion was run for over 60 iterations to reduce the rms residual traveltime from 95 ms for line 1 and 70 ms for line 3 to 11.4 and 11.2 ms, respectively. The resulting velocity models and ray coverage (Figures 6a, c) show penetration to 250–400 m depth, which is just enough to include the top-of-bedrock reflector in the seismic lines.

Because two different data sets were acquired along line 2, a slightly different approach to the inversion was taken for this profile. Initially, only the traveltimes from the first experiment were input into the inversion. After 30 iterations on these data, the rms traveltime residual for the starting model of 176 ms was reduced to 38 ms. The output velocity model was then adjusted at either end to remove edge effects attributable to low ray coverage. This reduced the rms traveltime residual to 32 ms. Traveltimes from the second experiment were then added to the observed data, and the inversion was allowed to run for an additional 26 iterations using the adjusted velocity model as a starting point. After 26 iterations, the rms traveltime residual had been reduced to 17.7 ms. The final velocity model and ray-coverage diagrams (Figure 6b) show that the addition of the

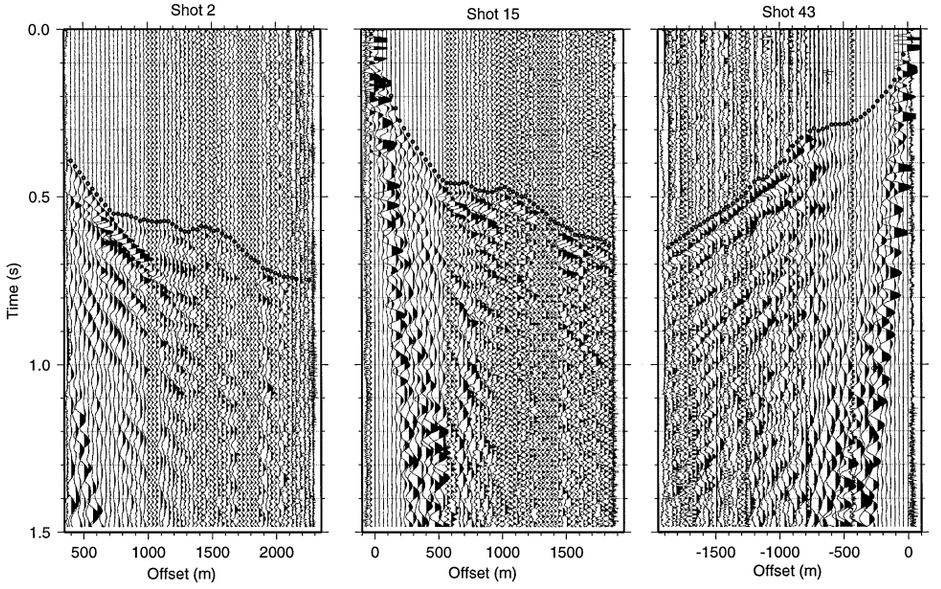

FIG. 5. Example shot gathers from the reoccupation of line 2, showing first-arrival picks (black circles). First arrivals were picked at the onset of a trough. On shot 15 at offsets of 800 to 1100 m, first arrivals are nearly flat, suggesting either extremely high-velocity material or a structure with high dip.

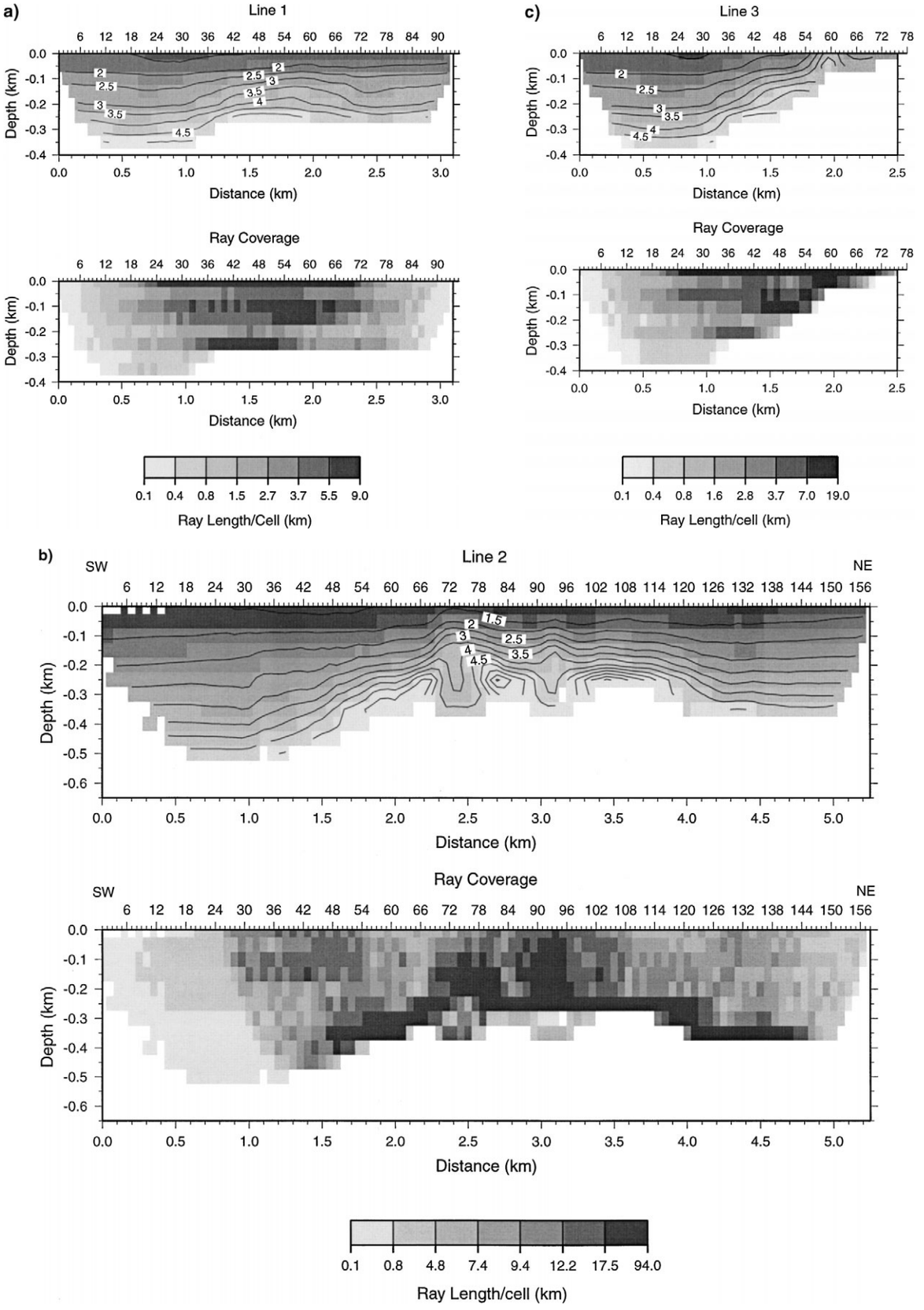

FIG. 6. Final velocity model and ray coverage for (a) line 1, (b) line 2, and (c) line 3. Vertical exaggeration is 2:1.

longer offset data from the second experiment increased the depth of ray coverage to 400–500 m compared to that on lines 1 and 3. By using this two-step approach, data from the first experiment became the primary constraint on velocities in the upper 200 m of the final velocity model. The addition of data from the second experiment led to changes in the deeper parts of the model but caused little adjustment to the near-surface velocities.

INTERPRETATION OF SEISMIC SURVEYS

An analysis of the diverse geological, geochemical, and geophysical data sets taken at the McGregor geothermal system permits an integrated and more rigorous interpretation of subsurface geology and dynamics of the geothermal system. Displays of the seismic results in which the velocity models and stacked seismic reflection records are superimposed (Figure 7) are effective interpretational tools. These were generated by converting the seismic record sections from time to depth using stacking velocity fields derived from smoothed versions of the final velocity models. Drill data from four core holes (Finger and Jacobson, 1997; Witcher et al., 1997), gravity models (this study), and resistivity models (Ross et al., 1998) were then used to complement the seismic interpretations.

Geometry of top of bedrock

The interpretation of the most prominent reflection on the seismic data as top of bedrock is supported by the velocity models and well data. All the seismic profiles show that a strong velocity gradient corresponds to the location of the reflector. Typically, velocities increase from 700 to 3000 m/s in the basin fill to 4000 to 6500 m/s in bedrock. The basin-fill–bedrock unconformity is represented by a strong velocity gradient rather than a discrete interface in the model because the tomography method can only produce smooth models. Importantly, the velocity models also help give a sense for topography at top of bedrock where reflections are absent or discontinuous.

That a bedrock high underlies the location of the gravity and heat-flow highs is most clearly demonstrated on line 2 (Figure 7b), where there is good ray coverage (Figure 6b) in the velocity model to an average depth of about 400 m. A strong velocity gradient from 3000 m/s to a maximum of 6500 m/s tracks the geometry of the strong reflector, corroborating the interpretation of this event as the top of bedrock. The velocity gradient defines a buried bedrock high with a high point of 150 m at the center of the line. To the northeast, the high velocities occur at a depth of 210 m; to the southwest, the high velocities do not occur until a depth of about 500 m. Thus, the seismic results suggest about 350 m of relief on the bedrock surface along line 2.

Deep ray coverage varies laterally from 350 to 550 m and is controlled by the depth to the high-velocity zone. At the center of the zone, rays penetrate only to 350 m but reach 550 m on the southwest end, where the bedrock reflector is much deeper. This variation occurs primarily because the rays are trapped in the high-velocity gradient at the top of bedrock. Just north of this profile, where the shallowest high-velocity zones are seen in the seismic data, well 45-5 encountered bedrock comprised of Mississippian limestones and shales at only 359 m.

Line 1 (Figure 7a), which lies almost entirely within the geothermal high (Figure 2), shows a bedrock high near 1.6 km of the profile at a depth of 180 m. That top of bedrock drops to depths as great as 350 m on either side of the high. This observation is consistent with data from well 61-6, which encountered felsic bedrock at 179 m depth. Velocities along the profile only reach 4000 m/s, suggesting that refracted energy either does not or just barely enters bedrock. The maximum depth of the ray coverage (Figure 6a) is only 300–350 m.

Line 3 (Figure 7c) exhibits similar relief on bedrock, much like that on line 2. As the line crosses into the geothermal anomaly, the bedrock reflector steps up from 400 m depth and approaches the surface near 2.1 km of the profile. High-velocity material nearly reaches the surface between shotpoints 60 and 66 and drops downward to the west. Bedrock crops out in the vicinity of shotpoint 66, supporting this interpretation.

Structures within bedrock

Careful examination of the relationship of the velocity model to the reflection data in the central portion of line 2 (Figure 7b) reveals that where the bedrock reflector becomes discontinuous, two 200- to 300-m-wide low-velocity anomalies occur within the shallow high-velocity zone. We interpret these low-velocity zones to represent water-filled zones of high permeability in the shallow bedrock caused by karsted bedrock, fracturing as the result of possible faulting, and solution-collapse breccia. A number of lines of evidence support this interpretation. The combined observation of average high velocity where the bedrock reflection breaks up suggests that the bedrock surface is too rough to image properly with the wavelengths present in the seismic data. A rough bedrock surface can be very characteristic of karst geomorphology (White, 1990). A long-lived geothermal system could also be expected to contribute to extensive hydrothermal karst and solution breccias in carbonate rocks (Bakalowicz et al., 1987). Major solution permeability was found in wells 45-5 and 46-6 in Pennsylvanian limestones near the static water table, above and below intrusive contacts, and near the bedrock–basin fill unconformity (Witcher, 1998). In addition, a cavernous interval was encountered in well 45-5 in Pennsylvanian rocks at 142 to 156 m depth. At the surface, a nearby topographic depression may indicate a sinkhole in basin fill over collapsing bedrock karst. Finally, the resistivity study along line 2 (Ross et al., 1998) shows a 3-ohm-m, low-resistivity zone near 200 m depth in the vicinity of the seismic low-velocity zones. Low electrical resistivities would be expected in the presence of conductive thermal fluids in zones of high porosity (Ross et al., 1998).

Reflections from within bedrock occur along the flanks of the bedrock high, but few occur beneath it. Taken together with well data, these observations suggest that intrusive rock may form the bedrock unconformity where few reflectors occur; where more intrabedrock reflectors are present, the bedrock unconformity is underlain by Paleozoic carbonate rocks, intruded by one or more sills. Well 61-6, situated on the bedrock high, encountered 250 m of felsite before entering Paleozoic sedimentary rocks. Less than a kilometer to the southwest, well 46-6 encountered Paleozoic bedrock at 209 m depth and then cored a 42-m-thick felsite sill at 349 to 391 m depth. In well 45-5, core shows strata dipping above the upper sill and flat strata at the base of this sill. The onlap geometry displayed by

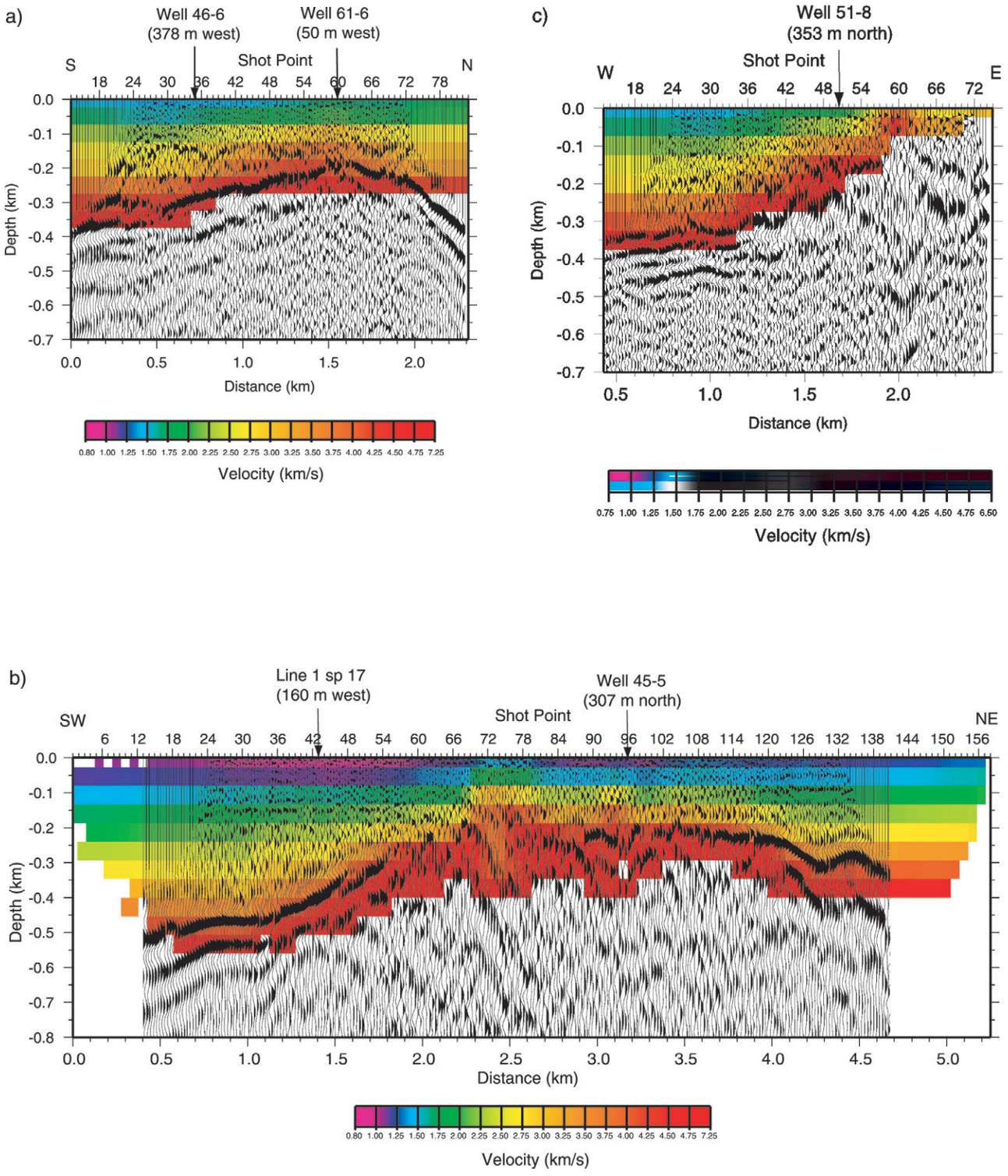

FIG. 7. Velocity model superimposed on depth-converted seismic reflection data for (a) line 1, (b) line 2, and (c) line 3. Vertical exaggeration is 2:1. Typically, velocities range from 700 to 3000 m/s in the basin fill to 4000 to 6500 m/s in bedrock. High velocities can be used to track the bedrock reflector, even where it becomes discontinuous. Reflections from the water table occur at 80 to 140 m.

intrabedrock reflectors north and south of the intrusive in the well 61-6 bedrock high appear to support a laccolith interpretation. Witcher (1998) interprets the felsic intrusion in wells 45-5, 46-6, and 61-6 as apophyses of a Christmas tree laccolith complex (Corry, 1988).

The well data illuminate other features of the bedrock geology. Wells 46-6 and 61-6 west of Davis Dome (Figure 2) encountered Mississippian limestones and shales at 525 and 531 m depth, respectively. Just south of Davis Dome, where the shallowest high-velocity zones are seen in the seismic data, well 45-5 encountered Mississippian limestones and shales at only 359 m. Felsite sills and a felsite laccolith of probable mid-Tertiary age were also cored by the wells. Well 45-5 encountered 378 m of felsite below the conformable Pennsylvanian and Mississippian contact. Well 46-6 to the west encountered no felsite below this contact. Well data indicate at least 170 m of offset on the Pennsylvanian and Mississippian contact. Felsite intrusions show at least 378 m of intrusive inflation difference in Mississippian strata among the wells. Because the regional dip of strata is to the east and south toward well 45-5, which has the greatest intrusive inflation, the 170 m of offset is easily reconciled by the difference in regional strata slope and local intrusive doming of a laccolith near well 45-5. Thus, the 350 m of west-dipping relief, defined by the bedrock reflector, is best interpreted as a buried erosional surface or unconformity on bedrock and may represent a range-front pediment buried by rapid late-stage basin-fill sedimentation after integration of the Rio Grande drainage into the area (Gustavson, 1991).

Of regional interest is a blind thrust fault that juxtaposes flat-lying Silurian dolomite on an overturned footwall of Mississippian black shale at 683 m depth, encountered 0.6 km north of of line 3 in well 51-8 (Witcher, 1998). The thrust fault may represent the shallow flattening of a major reverse fault on the vergent margin of a basement cored uplift (see Seager, 1983; Seager et al., 1986; Seager and Mack, 1986). The thrust fault may be slicing through a steep drape or monoclinal fold. A transpressional flower structure is also possible (see Cather, 1999). The age of this tectonism may be Late Paleozoic in association with the western margin of the Pedernal uplift and eastern Orogrande basin (Kluth, 1986), or it may be Late Cretaceous to Eocene age (Laramide Orogeny) (Seager, 1983). Outcrop and subsurface data for this structure are too scanty to infer more about its history.

Basin fill

Lateral changes in seismic velocity suggest changes in lithology within the basin fill, even though no reflections image the change. In the near surface of line 2, basin-fill velocities vary laterally from 700 m/s in the southwest to >1000 m/s to the northeast (Figure 7b). Geologic mapping (Figure 2) shows that Holocene eolian sands and Camp Rice Formation fluvial-channel sands occur near the surface on the southwest end of the line, and playa and alluvial-fan deposits shed from the Hueco Mountains occur on the northeast end. Higher velocities would be expected from alluvial-fan deposits since they not only contain high-velocity carbonate clasts but are also indurated from intervals of pedogenic carbonate (caliche) and diagenetic carbonate cements.

All three profiles feature wedges of intermediate-velocity material (3000–4000 m/s) in the deeper basin fill just above bedrock on the southwest flank of the bedrock high. This wedge of intermediate-velocity material may represent a Fort Hancock alluvial fan with limestone clasts derived from local bedrock. Alternatively, the higher velocity may result from moderate to strong cementation, typical of older Miocene basin-fill deposits in the region (Mack et al., 1998). Collins and Raney (1994) show an older package of basin-fill deposits in the Hueco basin interior that also has a good reflection signature. The Collins and Raney (1994) unit may correlate with our high-velocity basin fill; however, it more likely represents an older basin-fill unit found only in the main graben deposition center.

Water table

A single reflector, interpreted to be from the water table, consistently occurs within the basin fill at approximately 140 m depth on the southwest flank of the bedrock high (Figure 7). Support for this interpretation comes from well data which show that the top of the water table lies between 132 and 139 m. In addition, the reflector lies at a vertical transition in velocity from 1500 to 2000 m/s, an increase appropriate for a change from unsaturated to saturated sediments.

On line 2, the water-table reflection occurs at a depth of approximately 140 m on the southwest end of the line distance between 0.75 and 2 km east and then again at profile distance 3.5 and 4.5 km east at approximately 80 m depth to the northeast (Figure 7b). The reflector is not present above the bedrock velocity high; rather, it appears to dip down into it. One interpretation for the water table being higher on the northeast side of the profile than on the southwest is that the Pleistocene fault of Witcher (1998) (Figure 2) may be impeding water flow, causing alluvial-fan and playa recharge to pile up on the east footwall of the fault. Alternatively, the higher velocity fine-grained fan deposits may host perched and nonthermal water at a higher level because of low vertical permeability.

In any case, the water-table reflectors appear to dip into the shallow high-velocity bedrock zone on the Pleistocene fault footwall to the west, suggesting communication between the bedrock and basin-fill aquifers at this location. The implication is that water in the basin-fill aquifer is draining downward over the eastern margins of the shallow high-velocity zone in the vicinity of Davis Dome. These interpretations are consistent with the observation from deep well data that the geothermal fluids in the bedrock reservoir have a head about 30 m lower than coldwater heads in the basin fill. The head difference is even more pronounced if equivalent coldwater heads are compared between the two aquifers.

Continued solution collapse of the bedrock reservoir from geothermal fluids could be accompanied by sinkhole collapse into the overlying basin fill to create vertical fracture permeability across the low-permeability Fort Hancock deposits. Alternatively, the Pleistocene fault may have created vertical permeability to allow downward flow of perched water across the Fort Hancock Formation.

GRAVITY MODELING

Initially, a gravity survey served as part of the reconnaissance effort to define the overall structure associated with the geothermal system and to help site the seismic lines. Preliminary

gravity modeling helped to define the bedrock configuration beneath the basin fill. The gravity models presented here are constrained by the seismic reflection data and velocity models and are helpful for determining bedrock depth and geometry where unconstrained by the seismic data.

During the gravity survey, 148 gravity readings were taken along five profiles along strike and across the geothermal anomaly. The gravity measurements were spaced approximately 160 m apart along each profile. The data were reduced to Bouguer anomaly values (Cordell and Grauch, 1982) using an average crustal density of 2670 kg/m^3, a sea-level datum, and terrain corrections described by Plouff (1977). The new data were then merged with the 82 existing points in the study area (Keller and Cordell, 1983).

A residual gravity map (Figure 8) was generated from the merged data by removing a third-order polynomial surface from the Bouguer anomaly grid. This step removed the regional gravity anomaly from the data and left the local anomalies with possible control on the geothermal system. The residual map shows a southeast-to-northwest–trending gravity high that coincides with the heat-flow anomaly (Figure 8). The gravity high drops off by as much as 7 mGal to the northeast and southwest sides of the high. This pattern shows a local bedrock high that is associated with the higher heat-flow measurements.

A density model was generated from the gravity data along seismic line 2 using a forward modeling program based on the algorithm of Cady (1980). Initial density models were generated by assuming reasonable density contrasts and body geometries based on known geology. The density and shape of the bodies were then adjusted until the calculated anomaly matched the observed gravity data. Observed gravity values along each profile were filtered to remove the third-order polynomial before being input into the modeling program.

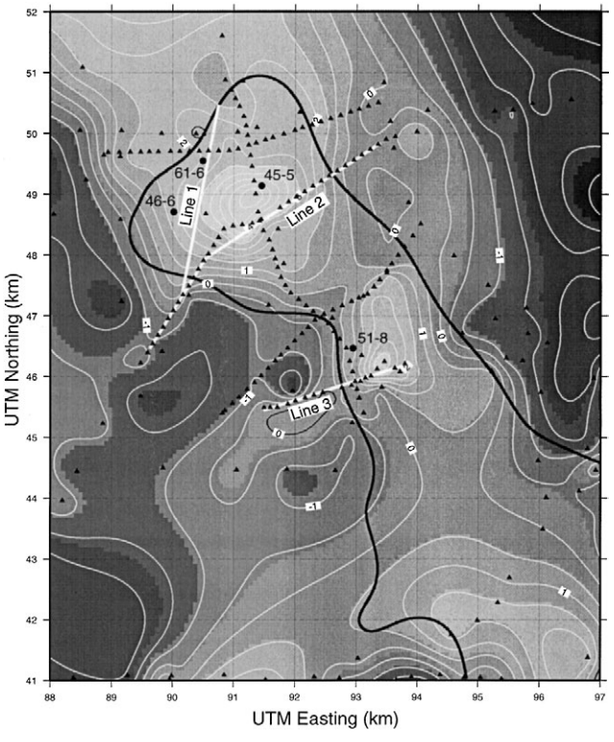

FIG. 8. Residual gravity map created by removing a third-order polynomial from the Bouguer gravity to remove regional effects. Contour interval is 0.5 mGal. Triangles are gravity stations, thick white lines are seismic lines, and large black circle are wells. The thick black line is the 400-mW/m^2 heat-flow contour. The gravity highs coincide with the heat-flow high.

Based on the stacked record section and the velocity model for line 2, a simple gravity model consisting of three bodies—low-density basin fill, higher density basin fill, and bedrock—was built (Figure 9). Bedrock densities for the felsic intrusives and different carbonate units were assumed to be similar.

The bedrock geometry was constrained by the seismic reflection data. The topography on the bedrock high came primarily from the velocity model (Figure 6b) because the reflection data lacked coherent reflectors in this region. To match the gravity, a third body, interpreted to be higher density basin fill on the west side of the bedrock uplift, was required. The geometry of the bodies, primarily constrained by seismic velocities, required only minor changes during the modeling process. A large density contrast between the basin fill and bedrock was required to obtain the 6-mGal change across the profile. A density value of 2600 kg/m^3 for the bedrock was chosen and is supported by the high velocities seen in the velocity model. A density value of 2000 kg/m^3 was chosen for the basin fill, and 2350 kg/m^3 was chosen for the higher density basin fill. These values were based on the density contrast required to generate the 6-mGal difference, since the depth to bedrock is well constrained by the seismic survey. The gravity model substantiates the bedrock high interpreted from the seismic data of line 2.

DISCUSSION AND CONCLUSIONS

The geological and geophysical data at the McGregor geothermal system suggest that it has many of the characteristics associated with convective geothermal systems in southern New Mexico as summarized by Witcher (1988). Among these characteristics are an association with low-elevation structural highs and a primary reservoir of high-permeability pre-Tertiary bedrock (Figure 10).

Analysis of the seismic and gravity data shows that the McGregor geothermal system is indeed associated with structurally high terrain. Igneous inflation from laccolith intrusion in early Tertiary time may have played the primary role in developing the structural high (Figure 10). Evidence for Pleistocene normal faulting exists on the eastern and western margins of the survey area, suggesting the structure is overprinted by a small and younger Pleistocene horst associated with the eastern hinge zone of the Hueco-Tularosa half-graben (Figure 10). Well 51-8 encountered a thrust fault and overturned footwall beds that indicate a previously unknown compressional structure of Late Cretaceous to early Tertiary or late Paleozoic age. This structure, along with fracturing during laccolith intrusion and late Tertiary normal faulting, probably all play an important role in creating deeply penetrating vertical fracture permeability for the geothermal system.

The bedrock low-velocity zones and lack of coherent reflectors point to the occurrence of high-permeability reservoir rocks within the bedrock high and suggest that permeable zones are most widespread nearest the bedrock–basin-fill unconformity. The bedrock highs seen in the seismic surveys and at Davis Dome may represent pre-Fort Hancock and Camp

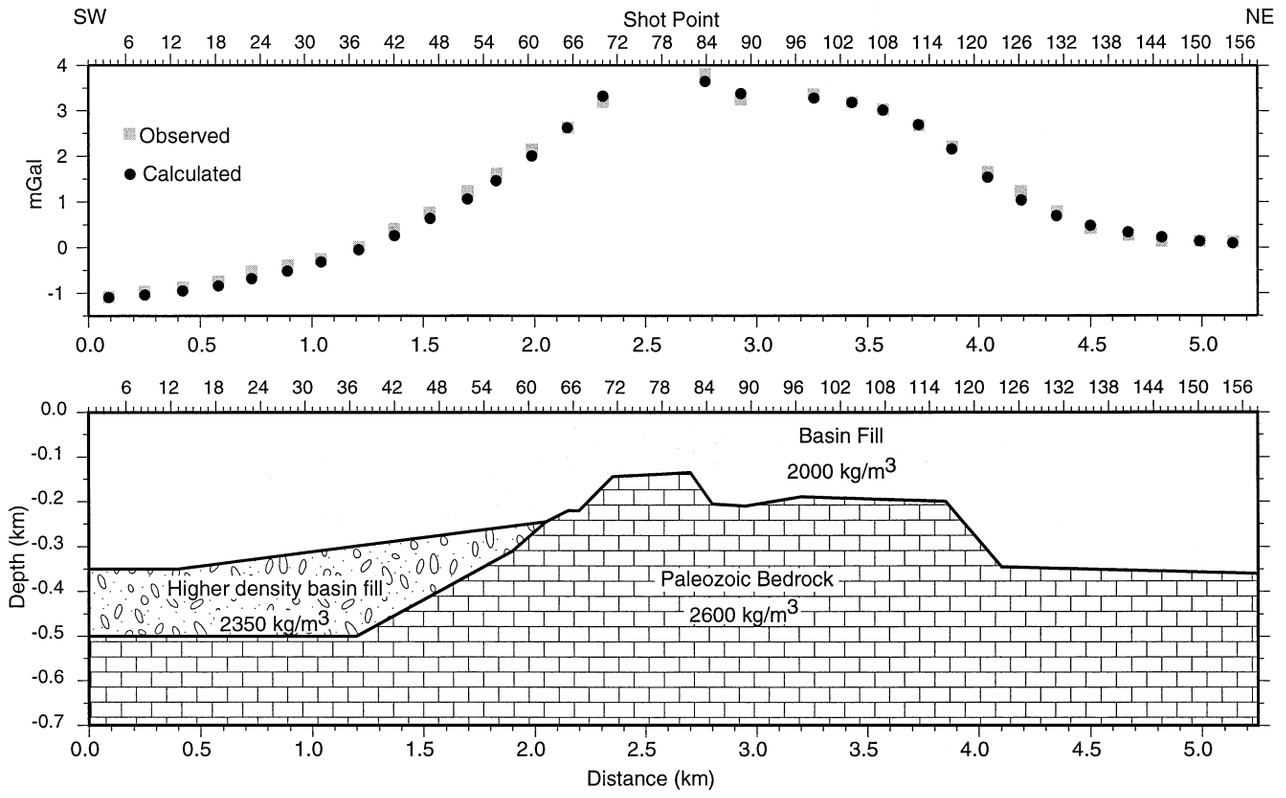

FIG. 9. Gravity model for line 2, showing a bedrock uplift (lower plot). Top plot compares the observed gravity to calculated gravity from the density model. The vertical exaggeration is 2:1.

Rice Formation pediment inselbergs and pediment erosional surfaces (Figure 2). The higher velocity and higher density fill on the west flank of the bedrock high may represent an earlier stage of basin fill or older Fort Hancock piedmont alluvial-fan deposits. The heat-flow anomaly appears to be constrained to the region of shallowest bedrock that lacks these deposits, suggesting that they may act as an aquitard to cap underlying bedrock aquifers or geothermal reservoirs.

Its low-elevation position west of the Hueco Mountains escarpment (Figure 1) suggests that differences in hydrostatic head probably drive the geothermal system. Recharge in the Hueco Mountains is forced by water-table head differences to circulate to great depth, where it is heated and then flows back toward the surface in the high-permeability bedrock beneath the survey area.

The seismic and gravity surveys provided key subsurface information needed to understand the dynamics and structural controls of the McGregor geothermal system. Measurements in test wells have shown that the thermal waters within the system have temperatures as high as 89°C. Integration of these results suggests that the site has potential for space heating, geothermal desalinization, and small-scale electrical production at McGregor Range.

ACKNOWLEDGMENTS

The U.S. Army Air Defense Artillery Center, Directorate of Public Works and Logistics at Ft. Bliss, Texas, provided funding to the University of Texas at El Paso for the seismic and gravity survey and to New Mexico State University for the other complementary geoscience surveys mentioned in this paper. Steve Harder of the University of Texas at El Paso planned and supervised all the seismic and gravity data acquisition. Ron Luna and Joe Mathis of Ft. Bliss assisted with logistics.

REFERENCES

Ammon, C. J., and Vidale, J. E., 1993, Tomography without rays: Seis. Soc. Am. Bull., **83**, 509–528.

Bakalowicz, M. M., Ford, D. C., Miller, T. E., Palmer, A. N., and Palmer, M. V., 1987, Thermal genesis of dissolution caves in the Black Hills, South Dakota: Geol. Soc. Am. Bull., **99**, 729–738.

Barrol, M. W., and Reiter, M., 1990, Analysis of the Socorro hydrogeothermal system, central New Mexico: J. Geophys. Res., **95**, 21 949–21 963.

Blair, T. C., Clark, J. S., and Wells, S. G., 1990, Quaternary continental stratigraphy, landscape evolution, and application to archeology: Jarilla piedmont and Tularosa graben floor, White Sands Missile Range, New Mexico: Geol. Soc. Am. Bull., **102**, 749–759.

Buck, B. J., Kipp, J. M., and Monger, H. C., 1998, Eolian stratigraphy of intrabasinal fault depressions in the northern Hueco and southern Tularosa basins: Evidence for neotectonic activity, *in* Mack, G. H., Austin, G. S., and Barker, J. M., Eds., Las Cruces country II: New Mexico Geol. Soc. 49th Ann. Field Conf. Guidebook, 79–86.

Cady, J. A., 1980, Calculation of gravity and magnetic anomalies of finite length right polygon prisms: Geophysics, **4**, 1507–1512.

Cather, S. M., 1999, Implications of Jurassic, Cretaceous, and Proterozoic piercing lines for Laramide oblique-slip faulting in New Mexico and rotation of the Colorado Plateau: Geol. Soc. Am. Bull., **111**, 849–868.

Collins, E. W., and Raney, J. A., 1994, Tertiary and Quaternary tectonics of Hueco bolson, Trans-Pecos Texas and Chihuahua, Mexico, *in* Keller, G. R., and Cather, S. M., Eds., Basins of the Rio Grande rift: Structure, stratigraphy, and tectonic setting: Geol. Soc. Am. Special Paper **291**, 265–281.

Cordell, L., and Grauch, J. S., 1982, Reconciliation of the discrete and

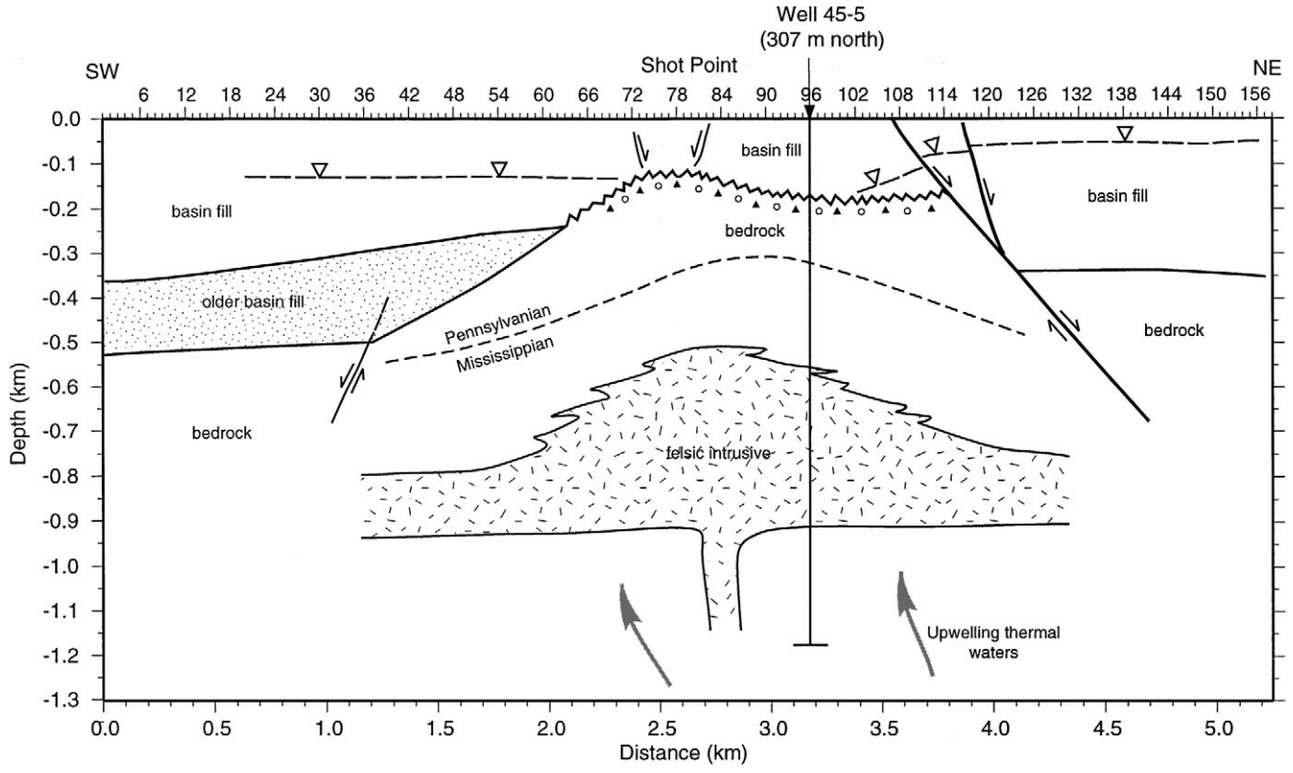

FIG. 10. Schematic of geology along line 2, based on an integration of all available data. Dashed line with triangles—water table; jagged line with triangles and circles—bedrock unconformity underlain by karsted bedrock. Vertical exaggeration is 2:1. High bedrock topography is probably the result of igneous inflation from laccolith intrusion during early Tertiary time. The structure is also overprinted by Pleistocene normal faulting. Deposits that flank the west side of the bedrock may represent an earlier stage of basin fill or older Fort Hancock piedmont alluvial-fan deposits. These flanking higher velocity zones appear to confine the highest heat flow to areas of shallow bedrock where solution-collapse breccias and cavities filled with hot water associated with karsted bedrock occur. The water table appears to dip into the bedrock high, suggesting communication between the bedrock and basin-fill aquifers.

integral Fourier transforms: Geophysics, **47**, 237–243.
Corry, C. E., 1988, Laccoliths: Mechanics of emplacement and growth: Geol. Soc. Am. Special Paper **220**.
Decker, E. R., and Smithson, S. B., 1975, Heat flow and gravity interpretations across the Rio Grande rift in southern New Mexico and West Texas: J. Geophys. Res., **80**, 2442–2552.
Finger, J. T., and Jacobson, R. D., 1997, Fort Bliss exploratory slimholes: Drilling and testing: Sandia Nat.'l Lab. Report **SAND97-3075**.
Gile, L. H., Hawley, J. W., and Grossman, R. B., 1981, Soils and geomorphology in the Basin and Range area of southern New Mexico—Guidebook to the Desert Project: New Mexico Bureau of Mines and Mineral Resources Memoir **39**.
Gile, L. H., Peterson, F. F., and Grossman, R. B., 1966, Morphological and genetic sequences of carbonate accumulation in desert soils: Soil Science, **101**, 347–360.
Gustavson, T. C., 1991, Arid basin depositional systems and paleosols: Fort Hancock and Camp Rice Formations (Pliocene–Pleistocene), Hueco bolson, West Texas and adjacent Mexico: Bur. Econ. Geol. Report of Investigations **198**.
Harder, V., Morgan, P., and Swanberg, C. A., 1980, Geothermal anomalies in the Rio Grande rift: Origins and potential: Geothermal Resources Council Transactions, **4**, 61–64.
Henry, C. D., 1979, Geologic setting and geochemistry of thermal water and geothermal assessment, Trans-Pecos Texas with tectonic map of the Rio Grande area, Trans-Pecos Texas and adjacent Mexico: Bur. Econ. Geol. Report of Investigations **96**.
Henry, C. D., and Gluck, J. K., 1981, A preliminary assessment of the geologic setting, hydrology, and geochemistry of the Hueco Tanks geothermal area, Texas and New Mexico: Bur. Econ. Geology Geological Circular **81-1**.
Hoffer, J. M. 1979, Geothermal exploration of western Trans-Pecos Texas: Texas Western Press.
Keller, G. R., and Cordell, L., 1983, Bouguer gravity map of New Mexico: Geothermal Resouces of New Mexico Scientific Map Series, 1:500 000 scale.
Kluth, C. F., 1986, Plate tectonics of the ancestral Rocky Mountains, *in* Peterson, J. A., Ed., Paleotectonics and sedimentation in the Rocky Mountain region: A.A.P.G. Memoir **41**, 353–369.
Lucia, F. J., 1988, Lower Paleozoic collapse brecciation and dolomitization, Franklin Mountains Tobosa basin related sequences: El Paso Geol. Soc. and Southwest Section A. A. P. G., 75–113.
Machette, M. N., 1985, Calcic soils of the southwestern United States, *in* Weide, D. L, Ed., Soils and Quaternary geology of the southwestern United States: Geol. Soc. Am. Special Paper **203**, 1–21.
——— 1987, Preliminary assessment of paleoseismicity at White Sands Missile Range, southern New Mexico: Evidence for recency of faulting, fault segmentation, and repeat interval for major earthquakes in the region: U.S. Geol. Surv. Open-File Report **87-444**.
Mack, G. H., Kotttlowski, F. E., and Seager, W. R., 1998, The stratigraphy of south-central New Mexico, *in* Mack, G. H., Austin, G. S., and Barker, J. M., Eds., Las Cruces country II: New Mexico Geol. Soc. 49th Ann. Field Conf. Guidebook, 135–154.
Mattick, R. E., 1967, A seismic and gravity profile across the Hueco bolson, Texas, *in* Geological Survey research 1967: U.S. Geol. Surv. Professional Paper **575-D**, D85–D91.
McLean, J., 1956, Saline groundwater resources of Tularosa basin, New Mexico: U.S. Geol. Surv. Office of Saline Water, Res. and Development Progress Report No. 561.
Morgan, P., 1989, Heat flow in the earth, *in* James, D. E., Ed., Encyclopedia of solid earth geophysics: Van Nostrand Reinhold, New York, 634–646.
O'Donnell, T. M., Jr., 1998, Integrated gravity and seismic reflection/refraction study of the McGregor geothermal system, southern New Mexico: MS thesis, Univ. of Texas at El Paso.
Plouff, D., 1977, Preliminary documentation for a Fortran program to compute gravity terrain corrections based on topography digitized

on a geographic grid: U.S. Geol. Surv. Open-File Report **77-535**.
Reiter, M., Edwards, C. L., Hartman, H., and Weidman, C., 1975, Terrestrial heat flow along the Rio Grande rift in New Mexico and southern Colorado: Geol. Soc. Am. Bull., **86**, 811–818.
Reiter, M., Eggleston, R. E., Broadwell, B. R., and Minier, J., 1986, Estimates of terrestrial heat flow from deep petroleum tests along the Rio Grande rift in central and southern New Mexico: J. Geophys. Res., **91**, 6225–6245.
Reiter, M., Mansure, A. J., and Shearer, C., 1979, Geothermal characteristics of the Rio Grande rift within the southern Rocky Mountain complex, *in* Riecker, R. E., Ed., Rio Grande rift: Tectonics and magmatism: Am. Geophys. Union, 253–267.
Reiter, M., Shearer, C., and Edwards, C. L., 1978, Geothermal anomalies along the Rio Grande rift: Geology, **6**, 85–88.
Ross, H. and Witcher, J. C., 1995, Self-potential survey, McGregor Range, Fort Bliss Military Reservation, New Mexico: Earth Sciences and Resources Institute, University of Utah, prepared for Southwest Technology Development Institute, New Mexico State University.
Ross, H. P., Mackelprang, C. E., and Witcher, J. C., 1998, Electrical resistivity survey, McGregor Range area, New Mexico: Energy and Geoscience Institute, University of Utah, prepared for Southwest Technology Development Institute, New Mexico State University.
Seager, W. R., 1980, Quaternary fault system in the Tularosa and Hueco basins, southern New Mexico and West Texas, *in* Dickerson, W., and Hoffer, J. W., Eds., Trans-Pecos region: New Mexico Geol. Soc. 31st Ann. Field Conf. Guidebook, 131–136.
——— 1983, Laramaide wrench faults, basement-cored uplifts, and complimentary basins in southern New Mexico: New Mexico Geology, **5**, 69–76.
Seager, W. R., and Mack, G. H., 1986, Laramide paleotectonics of southern New Mexico, *in* Peterson, J. A., Ed., Paleotectonics and sedimentation: A. A. P. G. Memoir **41**, 669–685.
Seager, W. R., and Morgan, P., 1979, Rio Grande rift in southern New Mexico, West Texas, and northern Chihuahua, *in* Riecker, R. E., Ed., Rio Grande rift: Tectonics and magmatism: Am. Geophys. Union, 87–106.
Seager, W. R., Hawley, J. W., Kottlowski, F. E., and Kelly, S. A., 1987, Geology of east half of Las Cruces and northeast El Paso 1×1 degree sheets, New Mexico: New Mexico Bur. Mines and Min. Resources Geol. Map 57, 1:100 000 scale.
Seager, W. R., Mack, G. H., Raimonde, M. S., and Ryan, R. G., 1986, Laramide basement-cored uplift and basins in south-central New Mexico, *in* Clemons, R. E., King, W. E., and Mack, G. H., Eds., Truth or Consequences region: New Mexico Geol. Soc. 37th Field Conf. Guidebook, 123–130.
Sinno, Y. A., Dagget, H., Keller, G. R., Morgan, P., and Harder, S. H., 1986, Crustal structure of the southern Rio Grande rift determined from seismic refraction profiling: J. Geophys. Res., **91**, 6143–6156.
Stuart, C. J., and Willingham, D. L., 1984, Late Tertiary and Quaternary fluvial in the Mesilla and Hueco bolsons, El Paso area, Texas: Sed. Geol., **38**, 1–20.
Taylor, B., 1981, Heat flow studies and geothermal exploration in western Trans-Pecos, Texas: PhD dissertation, University of Texas, El Paso.
Taylor, B., and Roy, R. F., 1980, A preliminary heat flow map of West Texas, *in* Dickerson, W., Hoffer, J. M., and Callender, J. F., Eds., Trans-Pecos region: New Mexico Geol. Soc. 31st Field Conf. Guidebook, 137–139.
Taylor, B., Roy, R. F., and Hoffer, J. M., 1980, Hueco Tanks: An initial evaluation of a potential geothermal area near El Paso, Texas: Geothermal Resources Council Transactions, **4**, 253–256.
Vidale, J. E., 1988, Finite-difference calculation of travel times: Seis. Soc. Am. Bull., **78**, 2062–2076.
——— 1990, Finite-difference calculation of travel times in three dimensions: Geophysics, **55**, 521–526.
White, W. B., 1990, Surface and near-surface karst landforms, *in* Higgins, C. G., and Coates, D. R., Eds., Groundwater geomorphology: Geol. Soc. Am. Special Paper **252**, 157–175.
Witcher, J. C., 1988, Geothermal resources of southwestern New Mexico and southeastern Arizona, *in* Mack, G. H., Lawton, T. F., and Lucas, S. G., Eds., Cretaceous and Laramide tectonic evolution of southwestern New Mexico: New Mexico Geol. Soc. 39th Ann. Field Conf. Guidebook, 191–197.
——— 1998, Geothermal resource potential of McGregor Range, New Mexico: New Mexico State University/Southwest Technology Development Institute Report **GEO-97-5**.
Witcher, J. C., Davis, B. T., Furrick, B. J., and Stepro, M. W., 1997, Geologic analysis of core and geophysical logs from four slim-hole geothermal test holes, McGregor Range, Ft. Bliss, New Mexico: New Mexico State University/Southwest Technology Development Institute Report **GEO-3-97**.
Woodward, L. A., Callender, J. F., Seager, W. R., Chapin, C. E., Gries, J. C., Shaffer, W. L., and Zilinski, R. E., 1978, Tectonic map of Rio Grande rift region in New Mexico, Chihuahua and Texas, *in* Hawley, J. W., Ed., Guidebook to Rio Grande rift in New Mexico and Colorado: New Mexico Bur. Mines and Min. Res. Circular **163**.